Final Draft
of the original manuscript:

Liu, Y.; Razzaq, M.Y.; Rudolph, T.; Fang, L.; Kratz, K.; Lendlein, A.:
Two-Level Shape Changes of Polymeric Microcuboids Prepared from Crystallizable Copolymer Networks.
In: Macromolecules. Vol. 50 (2017) 6, 2518 - 2527.
First published online by ACS: 13.03.2017

https://dx.doi.org/10.1021/acs.macromol.6b02237

Two-Level Shape Changes of Polymeric Microcuboids Prepared From Crystallizable Copolymer Networks

Yue Liu[+,#], Muhammad Yasar Razzaq[+], Tobias Rudolph[+], Liang Fang[+,§], Karl Kratz[+], and Andreas Lendlein[+,#,*]

[+] Institute of Biomaterial Science and Berlin-Brandenburg Center for Regenerative Therapies, Helmholtz-Zentrum Geesthacht, Kantstr. 55, 14513 Teltow, Germany

[#] Institute of Chemistry, University of Potsdam, 14476 Potsdam, Germany

[§] Present address: State Key Laboratory of Materials-Oriented Chemical Engineering, College of Material Science and Engineering, Nanjing Tech University, 210009 Nanjing, China

*Corresponding author:

Prof. Andreas Lendlein

Institute of Biomaterial Science and Berlin-Brandenburg Center for Regenerative Therapies, Helmholtz-Zentrum Geesthacht, Kantstr. 55, 14513 Teltow, Germany

Phone: +49-(0)3328 – 352 450

Fax: +49-(0)3328 – 352 452

E-mail address: andreas.lendlein@hzg.de

Abstract

Polymeric microdevices bearing features like nonspherical shapes or spatially segregated surface properties are of increasing importance in biological and medical analysis, drug delivery, bio-imaging or microfluidic systems as well as in micromechanics, sensors, information storage or data carrier devices. Here, a method to fabricate programmable microcuboids with shape-memory capability and the quantification of their recovery at different levels is reported. The method uses the soft lithographic technique to create microcuboids with well-defined sizes and surface properties. Microcuboids having an edge length of 25 μm and a height of 10 μm were prepared from crosslinked poly[ethylene-*co*-(vinyl acetate)] (cPEVA) with different vinyl acetate contents and were programmed by compression with various deformation degrees at elevated temperatures. The microlevel shape-recovery of the cuboidal geometry during heating was monitored by optical microscopy (OM) and atomic force microscopy (AFM) studying the related changes in the projected area (PA) or height, while the nanolevel changes of the nanosurface-roughness were investigated by in-situ AFM. The shape-memory effect at micro-level was quantified by the recovery ratio of cuboids ($R_{r,micro}$), while at nanolevel, the recovery ratio of the nanoroughness ($R_{r,nano}$) was measured. The values of $R_{r,micro}$ could be tailored in a range from 42 ± 1% to 102 ± 1% and $R_{r,nano}$ from 89 ± 6% to 136 ± 21% depending on the applied compression ratio and the amount of vinyl acetate content in the cPEVA microcuboids.

Keywords: switchable microobjects; shape-memory polymers; stimuli-responsive materials; nano-roughness

1. Introduction

The design of complex shape changing microobjects is a challenging and yet highly important task, as active microobjects are needed in controlled drug delivery, sensors and microfluidic systems.[1-10] Numerous stimuli-sensitive polymers such as hydrogels,[11] liquid crystalline elastomers[1,2] or electroactive polymers[3] have been downscaled to generate micro- or nanoscaled objects. The shape change maneuvers of these microobjects could be controlled by different external stimuli, *e.g.,* heat,[12] light,[13] water,[14] pH[15] or electric field.[16] Thermally-induced shape-memory polymers (SMPs) with their unique capability to recover to their original geometries from programmed temporary shapes, when a characteristic temperature is reached, are promising candidates to generate switchable microobjects or miniaturized biomedical devices.[17-27] A prerequisite to observe a shape-memory effect (SME) in these microobjects are specific thermomechanical programming and characterization procedures at microscale level. Furthermore, the choice of the polymer, surface chemistry, and shape of the particles are important parameters to control the functional behavior of these microobjects. So far, one-way and reversible shape-memory effects have been described for spherical polymeric microparticles.[4,28,29] However, the precise characterization of the shape changing microparticles is a challenge due to their spherical shape, which makes it difficult for proper investigation by microscopic analysis caused by changing focus depths. Also, the visualization by AFM is limited because of the curvature of the particle surface. Furthermore, the uniformity in shape and size of the spherical particles can vary resulting from the fabrication methods such as emulsion polymerization or microfluidic procedures.[6,30] Therefore, nonspherical shapes with on-demand actuation capability would be desired. Recently, nonspherical microobjects based on surface functionalized polyesters with a potential value in the biomedical field have been described.[31] However, a complex multi-step programming procedure was used to achieve the temporary shape of the microobjects. Besides switchable macroscopic objects, smart surfaces

comprising nanofeatures are of special interest in the field of nanotechnology for controlling their physical properties. Here, controlling the nanosurface roughness allows the tuning of *e.g.*, bacterial adhesion[32] or wettability[33] or catalytic area[34] of objects. Microcuboids, having different faces, have been tailored with various chemical functionalities or surface roughness, offering a side/face specific biological interaction.[35] These cuboidal geometry can be used to tune the solution properties and flow behavior of particle suspensions.[36] Furthermore, nano-structured programmable microobjects might be of outstanding interest for coding and encoding of information on different length scales.

In this work, we explored the shape-memory performance of microcuboids prepared from crosslinked polymer networks with crystallizable switching units. Our strategy was to use soft lithography technique to prepare microcuboids of defined sizes and shapes as well as different nanostructured faces. We speculated that these microcuboids can be programmed by applying different compression ratios using a specific programming procedure and a micro- and nano-level recovery behavior of microcuboids, including, i) microscaled recovery of cuboidal geometry, and ii) recovery of the nanoscaled surface roughness, can be investigated.

To check the feasibility of our concept, microcuboids based on crosslinked poly[ethylene-*co*-(vinyl acetate)] (cPEVA) consisting of crystallizable polyethylene (PE) switching domains and amorphous poly(vinyl acetate) (PVA) domains were fabricated using the soft lithographic method. Crosslinking of the linear PEVA was carried out by using dicumyl peroxide (DCP) as thermal initiator. To further tailor the elastic properties and actuation temperatures, cPEVA with two different vinyl acetate contents were used. Individual microcuboids were programmed by compression with different deformation degrees and their shape-memory properties were evaluated. The temperature-induced microlevel recovery of the compressed single micro-cuboids was recorded online by optical microscopy (OM), where the changes in the projected

area (*PA*) were followed, while the changes in the microcuboid´s height (*H*) and the nanolevel surface roughness were investigated by *in situ* atomic force microscopy (AFM).

2. Experimental Section

2.1 Preparation of PDMS and PEVA/DCP film: A poly(dimethylsiloxane) (PDMS) soft mold replicate of the microstructured Si-wafer (IMS CHIPS, Stuttgart, Germany) was synthesized from a precursor mixture of 90 wt% prepolymer Sylgard ® 184 and 10 wt% curing agent (Dow Corning Corp., Midland, USA) by curing at 80 ºC for 24 hours. The achieved microstructured PDMS mold was utilized as negative template for fabrication of a second PDMS soft mold comprising micro-wells following the aforementioned procedure. The resulting PDMS mold was applied for generation of microstructured crosslinked cPEVA intermediate thin films. A mixture of 0.228 g of poly[ethylene-*co*-(vinyl acetate)] with vinyl acetate contents of 18 wt% (PEVA18) or 40 wt% (PEVA40) (DuPont de Nemours, Neu-Isenburg, Germany) and 4.6 mg of DCP (Sigma-Aldrich Chemie GmbH, Taufkirchen, Germany) was dissolved in 50 mL of toluene overnight at 60 °C. The prepared solution was casted in glass Petri dishes (diameter = 80 mm, Duran Group, Wertheim, Germany), and the solvent was subsequently evaporated for 5 days until constant weight was reached. The resulting PEVA/DCP film thickness was 30 ± 3 µm as determined by a thickness gauge (Hans Schmidt, Waldkraiburg, Germany).

2.2 Microcuboid preparation: The PEVA/DCP film was placed on the microwell-structured PDMS mold, and the sandwich was covered from both sides with a microscopy glass slide (25 mm × 75 mm) and a weight of 500 g on top. By heating to 130 ºC for 5 minutes the PDMS microcavities should be completely filled with PEVA/DCP for 5 min. After unloading, the remaining PEVA/DCP film on the surface of PDMS mold was removed with a tweezer. For crosslinking of the remaining PEVA/DCP mixture in the cuboidal microcavities the PDMS

mold was covered again with a microscopy glass slide and heated to 200 °C for 30 min, according to the method described in reference[12]. Afterward, the filled PDMS mold was cooled first to ambient temperature and finally stored at 5 °C in a refrigerator (Vitacool, Foron, Scharfenstein, Germany) for 20 min to allow complete crystallization of the cPEVA micro-cuboids. Finally, the microcuboids were transferred from the PDMS mold to a glass slide. Before further investigation, the prepared microcuboids were heated above melting temperature (100°C for cPEVA18 and 70°C for cPEVA40) for 20 min to remove thermal history and internal stress induced from crosslinking reaction.

2.3 Gel content (G): For determination of *G*, test specimens of cPEVAs were immersed in ca. 20 mL of toluene in glass vials and kept for 24 hours at 80 ºC in an oven. Afterward, the swollen samples were dried on the hot plate (PRÄZITHERM, Harry Gestigkeit GmbH, Düsseldorf, Germany) for 5 hours at 80 ºC until a constant weight was reached (m_d). The gel content (G) was calculated as the quotient of the mass of the dried samples after extraction (m_d) to the mass of the original samples (m_{iso}) (Eq. 1). For each type of cPEVAs, three specimens were investigated.

$$G\% = \frac{m_d}{m_{iso}} \times 100\% \quad (1)$$

2.4 Differential Scanning Calorimetry: Differential Scanning Calorimetry (DSC) experiments were conducted on a Netzsch DSC 204 Phoenix (Selb, Germany) at heating and cooling rates of 10 K·min^{-1} in sealed aluminum pans. A typical testing cycle is described in the following. The polymer samples were first heated from room temperature to 150 ºC before it was cooled down to -100 ºC. Subsequently, the sample was reheated to 150 ºC. The crystallization temperatures (T_c), melting temperatures (T_m), and the related melting enthalpies (ΔH) were determined from the second cooling and heating runs.

The crystallinity of both polymers was estimated by the following equation:

$$\text{crystallinity (\%)} = \frac{\text{melting enthalpy of sample}}{\text{melting enthalpy of 100\% PE (290 J·g}^{-1}\text{)}} \quad (2)$$

2.5 Dynamic Mechanical Thermal Analysis: Dynamic mechanical thermal analysis (DMTA) measurement was carried out on an Eplexor 25 N (Gabo, Ahlden, Germany) equipped with a 25 N load cell using the standard type test specimen (DIN EN ISO 527-2/1BB). The applied oscillation frequency was 10 Hz. The measurement was performed in the temperature sweep mode from -100 °C to 150 °C with a constant heating rate of 2 °C·min^{-1}. The glass transition (T_g) was determined at the peak maximum of loss factor (tan δ) *vs* temperature curve.

2.6 Programming of microcuboid: Programming of the cPEVA cuboids (25 × 25 × 10 μm^3) for dual-shape effect quantification was conducted by compression at 100 °C for cPEVA18 and 70°C for cPEVA40. First, the microscopy glass slide containing the transferred micro-cuboids was pre-heated for 10 min at 100 °C for cPEVA18 and 70 °C for cPEVA40 in a thermo-oven (Vacutherm, Heraeus, Hanau, Germany); afterward, a second microscopy glass slide was placed on top, two foldback clips (width 25 mm) were mounted on the equipment for compression, and the whole programming setup was equilibrated at 100 °C for cPEVA18 and 70°C for cPEVA40 for 20 min in the thermo-oven. The force of the applied foldback clips was measured by stretching the two sides to leave the gap as 2 mm equivalent to the thickness of two glass slides and was determined as 20 N. Afterwards the set-up was cooled first to ambient temperature and finally stored at 5 °C in a refrigerator for 20 min to allow fixation of der compressed temporary shape by crystallization. Finally, the foldback-clips and the top cover slide were subsequently removed and programmed microcuboids placed on a microscopy glass slide were achieved.

2.7 Microscopy analysis: The prepared single microcuboids as well as the temperature-induced shape change of single compressed microcuboids were investigated by optical microscopy (OM) and atomic force microscopy (AFM). While 50 microcuboids were investigated in OM for characterization of the thermally treated original microcuboids, the

shape recovery behavior was investigated for individual microcuboids. Optical micrographs were captured by a digital optical microscope (VHX-100K, Keyence Cor., Osaka, Japan). For temperature dependent measurements in a temperature range from 25 to 60 °C a warm microscopy stage type THN/A/O 60 (Linkam Scientific Instruments, Tadworth, UK) was applied to monitor the shape changes online. A precision hot plate PZ 28-2 (Harry Gestigkeit GmbH, Düsseldorf, Germany) was utilized for exposure of the microcuboids to temperatures ranging from 60 to 100 °C, while the OM images were taken afterward (off-line) at 60 °C with warm microscopy stage. In both cases each temperature was equilibrated for 10 min. The systematic error of temperature control was ± 2 °C. The projected area (*PA*) of the cuboids in the obtained OM images was analyzed by software ImageJ 1.46r (NIH, USA). The measurement error was estimated to ± 10 μm^2.

The average height of microcuboids before programming (N = 50) and the individual height of single microcuboids after deformation at different programming conditions were investigated by AFM on a MFP-3D (Asylum Research, Santa Barbara, CA, USA). A silicon cantilever (OLYMPUS OMCL AC200TS-R3) having a driving frequency of around 150 kHz and a spring constant of 9 $N \cdot m^{-1}$ was utilized at typical scan rates between 0.5 and 0.75 Hz. The scan size of microgeometry change was between 50 to 70 μm. The scan size of nano-roughness change was chosen from central part (10 × 10 μm^2) of the cuboid surface. *In situ* AFM measurements of individual cuboids were conducted in the dry state where the temperature was controlled in the range from 25 to 100 °C by an environmental controller (Asylum Research, Santa Barbara, CA, USA) after equilibrating the sample for 10 min. The systematic error of temperature control was ± 2 °C.

2.8 Kinetic investigation of shape recovery: For kinetic investigations an array of programmed microcuboids (in this case with a dimension of 100 x 100 x 10 μm^3) at elevated temperature (i.e., 100 °C) was used. Here a heating plate (model PZ 28-2, Harry Gestigkeit

GmbH, Düsseldorf, Germany) was directly mounted below the microscope equipped with a high-speed camera for recording (model VW-9000E, KEYENCE Deutschland GmbH, Neu-Isenburg, Germany). For a better heat transfer through the supporting substrate to the micro-cuboids aluminum foil was utilized as substrate. For analysis the projected area was determined by software ImageJ 1.46r (NIH, USA) at different time steps for 3 particles. For fitting the respective data points an expanded exponential plot with respect to equation (3) was used. The time-dependent (t) decay of the data points can be determined in a term in which A, B, and C are individual variables and τ represents the decay of the system:

$$\mathrm{G(t)} = A + B\exp\left(-\frac{t}{\tau}\right) + Cexp\left(-\frac{t}{\tau}\right) \quad (3)$$

3. Results and Discussion

Crosslinked poly[ethylene-*co*-(vinyl acetate)] (cPEVA) with a vinyl acetate content of 18 wt% (cPEVA18) and 40 wt% (cPEVA40) enabled a broad melting transition in the temperature interval related to crystalline polyethylene domains and exhibited excellent shape-memory properties.[12] Generally, soft lithography methods allow the preparation of microobjects with well-defined structures, whereby additionally the nanotopography of the microobjects' surfaces can be controlled.[31,35] Therefore, a soft poly(dimethylsiloxane) (PDMS) mold approach was chosen for fabrication of cPEVA microcuboids having an edge length of 25 µm and a height of 10 µm (for a detailed description see the experimental section). Before the investigation of the SMEs of cPEVA microcuboids, it is important to determine their physical properties.

3.1 Characterization of cuboidal microparticles

First of all, the conversion of the crosslinking reaction and the crosslink density were investigated by swelling experiments on bulk material (film) with the same chemical composition. The gel content (G) of cPEVA rises from 89% to 97% with increasing vinyl acetate content from 18 wt% to 40 wt%, which indicates that cPEVA40 reached a higher

conversion in crosslinking reaction. To see the thermal transitions, differential scanning calorimetry (DSC) was carried out. Because of the high number of microcuboids which would be needed for an accurate DSC measurement, DSC was performed with intermediate micro-structured cPEVA films. Such films had an overall thickness around 30 μm. **Figure 1** shows the broad melting temperatures (T_m) for cPEVA18 and cPEVA40 with a peak maximum at 82 ± 1 °C and 42 ± 1 °C, respectively. Based on the thermal transitions, the deformation temperatures (T_{deform}s) were chosen as 100 °C for cPEVA18 and 70 °C for cPEVA40, which are above the broad melting transition of PE segments to achieve a complete melting of PE crystals before programming (**Table 1**).

Furthermore, to investigate the thermomechanical behavior, dynamic mechanical thermal analysis (DMTA) at varied temperatures was carried out (**Figures 1B and C)**. For cPEVA18, the loss factor *tan δ* peak ranging from -50 °C to 30 °C was attributed to a broad glass transition of the amorphous phase. (**Figure 1B**). On the other hand, cPEVA40 with a higher VA content resulted in a relatively sharp *tan δ* peak (-40 °C to 20 °C). Furthermore, a significantly lower value of *tan* δ_{max} = 0.27 (at -8 °C) for cPEVA18 as compared to cPEVA40 *tan* δ_{max} = 0.71 (at -18 °C) was observed. The changes in storage modulus E' in a temperature range from -100 °C to 100 °C are shown in **Figure 1C**. Below the start of glass transition at -40 °C, an almost similar value of $E' \approx 1424$ MPa for both cPEVAs was observed. With increasing the temperature, both samples showed an inflection point in a broad temperature range, which was affected by the overall crystallinity of the samples. For cPEVA40, the transition was ended at ~ 70 °C with a plateau value of $E' = 2.51$ MPa, while for cPEVA18, it continued up to 100 °C, resulting in E' of 2.75 MPa. These differences in the loss modulus and storage modulus would affect the deformation capability of both compositions. The thermal and morphological properties of both cPEVA samples are provided in Table 1.

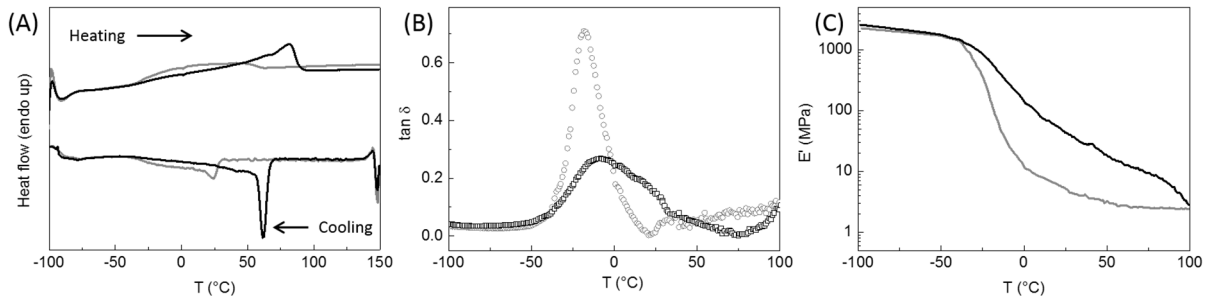

Figure 1: (A) DSC thermograms (2nd heating and 1st cooling runs) of cPEVA18 (black) and cPEVA40 (grey) films. Changes in loss factor, *tan δ* (B) and storage modulus, *E′* (C) with temperature determined by DMTA measurements of cPEVA18 (black) and cPEVA40 (grey) films.

Table 1. Physical properties of cPEVA18 and cPEVA40 intermediate films obtained from DSC, DMTA and gel content measurements.

Samples	$T_{m,onset,PE}$[a] [ºC]	$T_{m,offset,PE}$[a] [ºC]	$\Delta H_{m,PE}$[a] [J·g^{-1}]	$T_{c,PE}$[a] [ºC]	$T_{g,PE}$[b] [ºC]	G[c] [%]
cPEVA18	20 ± 1	94 ± 1	62 ± 2	60 ± 1	-8 ± 1	89 ± 1
cPEVA40	-10 ± 1	62 ± 1	25 ± 2	22 ± 1	-17± 1	97 ± 1

[a] obtained from DSC measurement; [b] obtained from DMTA measurement. [c] determined by swelling experiments.

A schematic illustration of the two-level programming and recovery of the cuboids at micro-level and the surface-roughness at nanolevel is shown in **Scheme 1**. To erase the thermal history or any internal stress generated during the crosslinking process, the cuboids were heated above the respective T_m of the polymer before further investigations. The illustrated original surface roughness of the microobjects is induced by the etched silicon wafer used for the fabrication of the mold. Microscopic investigations of the fabricated microcuboids were carried out by optical microscopy (OM) and atomic force microscopy (AFM). Optical images confirmed a uniform shape and geometry of the cuboids (**Figures 2A, D**). AFM results revealed an excellent uniformity of the achieved microcuboids having an average height of H = 10.8 ± 0.4 µm for cPEVA18 and H = 10.5 ± 0.3 µm cPEVA40 (AFM), while a mean projected area (PA) was *PA*

= 531 ± 18 µm^2 for cPEVA18 and *PA* = 588 ± 23 µm^2 for cPEVA40. The decrease in the *PA* compared to the theoretically predicted value of 625 µm^2 could be attributed to the crosslink induced contraction /shrinkage of the microcuboids. Such high crosslinking values have been confirmed by high values of *G* during swelling experiments (**Table 1**).

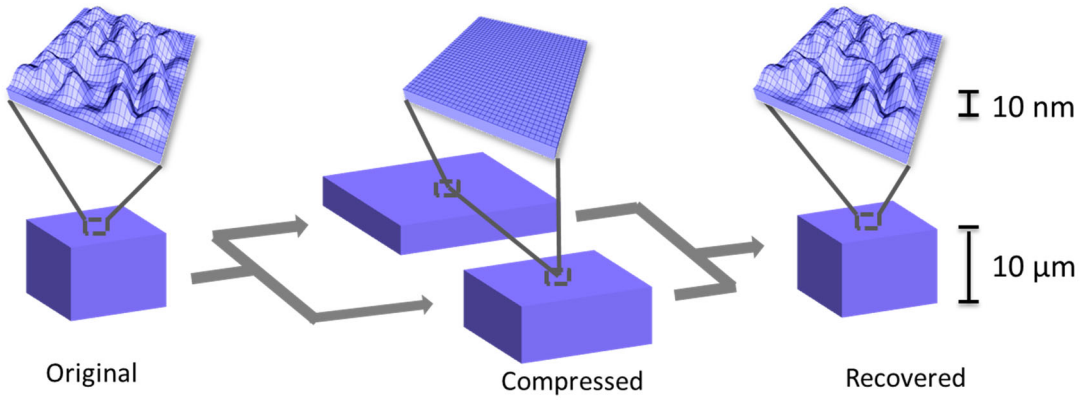

Scheme 1: Schematic representation of the two-step programming and recovery of the cuboidal geometry at the microlevel and the surface roughness at the nanolevel.

In **Figure 2** representative OM images and AFM height images of a single microcuboid and related 3D height images are displayed. **Figures 2C** and **2F** furthermore depict the roughness of the surface in the center of the cuboids obtained by AFM. The respective roughness values calculated for cPEVA18 and cPEVA40 are 17 ± 1 nm and 19 ± 1 nm, which are almost identical to the roughness of microwell surface of the PDMS template.

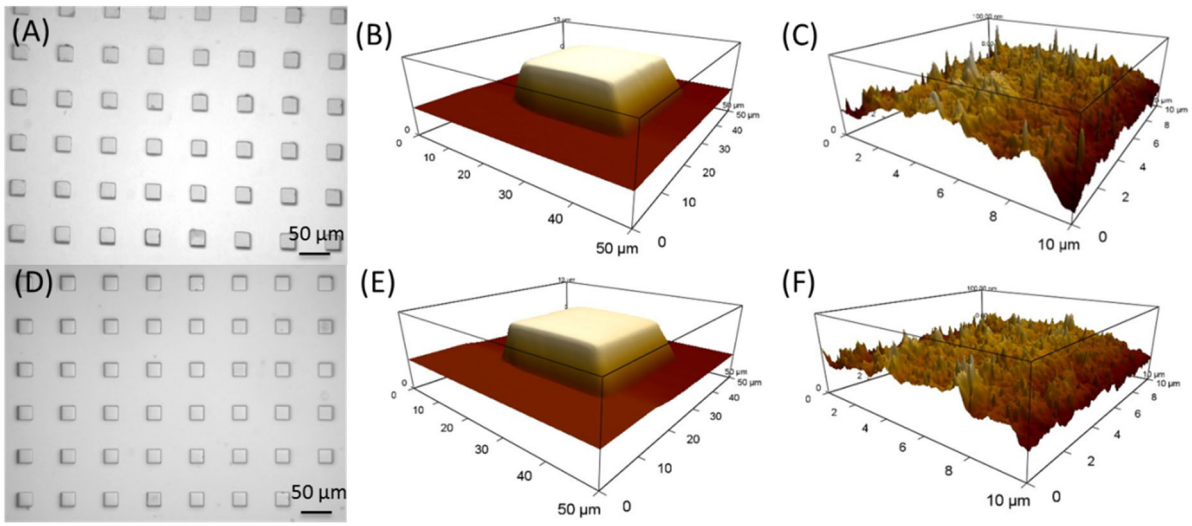

Figure 2: (A, D) Optical microscopy images of cPEVA18 (A) and cPEVA40 (D) micro-cuboids placed on a glass slide obtained with a magnification of 500×. (B, E) AFM height images of a single microcuboid of cPEVA18 (B) and cPEVA40 (E). The contrast of height image is represented from -10 µm to 10 µm; (C, F) AFM height images of cPEVA18 (C) and cPEVA40 (F) microcuboids top surface center.

3.2 Micro shape-memory capability

The thermal and thermomechanical investigations were followed by shape-memory investigations of the microcuboids. Common programming procedures for microparticles are the stretching of the soft macroscopic PDMS mold filled with particles, which has been utilized for preparation of nonspherical particles with diverse shapes[31] or elongation of a poly(vinyl alcohol) film containing the spherical shape-memory polymer microparticles, whereby the film was dissolved after completion of programming for harvesting the deformed particles.[28,37] In the current study, a simple and solvent free process was used for the programming of the micro-cuboids. Such a process involves compression of the microobjects between two glass slides at 100 °C (for cPEVA18) or 70 °C (for cPEVA40), where cPEVA is in the completely amorphous state, and the deformed shape was afterward fixed by the polyethylene crystallites formed during cooling to 5 °C. The obtained programmed microcuboids exhibited different deformation levels as shown in **Figures 3A** and **B**. The degree of deformation in height on the microlevel can be characterized as the microcompression ratio *CR*, which is defined by the ratio of the deformed, temporary fixed height H_u to the nondeformed original height H_0 of the microcuboids determined by AFM, and can be calculated from the following equation (4). Here, the apparent heights are $H_o = V/PA_o$ and $H_u = V/PA_u$, assuming a constant volume (V) of the microcuboids.

$$CR=\left(1-\frac{H_u}{H_0}\right)\cdot 100\% \quad \text{or} \quad CR=\left(1-\frac{V/PA_u}{V/PA_0}\right)\cdot 100\% \qquad (4)$$

The obtained different *CR* values, i.e., 27 ± 4% (CR_{27}), 42 ± 1% (CR_{42}), 66 ± 1% (CR_{66}), and 75 ± 1% (CR_{75}) for cPEVA18 as well as 23 ± 4% (CR_{23}), 44 ± 1% (CR_{44}), 73 ± 1% (CR_{73}), and 79 ± 1% (CR_{79}) for cPEVA40, which are represented by different *PA*s, can be attributed to a nonuniform force distribution to the cPEVA microcuboids at different places of the microscopy slides during the programming procedure. Respective OM and selected AFM images of the programmed/compressed samples are displayed in **Figure 3**. Height profiles of the cPEVA18 and cPEVA40 cuboids at different compressions show similar heights at comparable *CR*s, indicating a similar programmability of both cPEVAs (**Figures 3 G, H**).

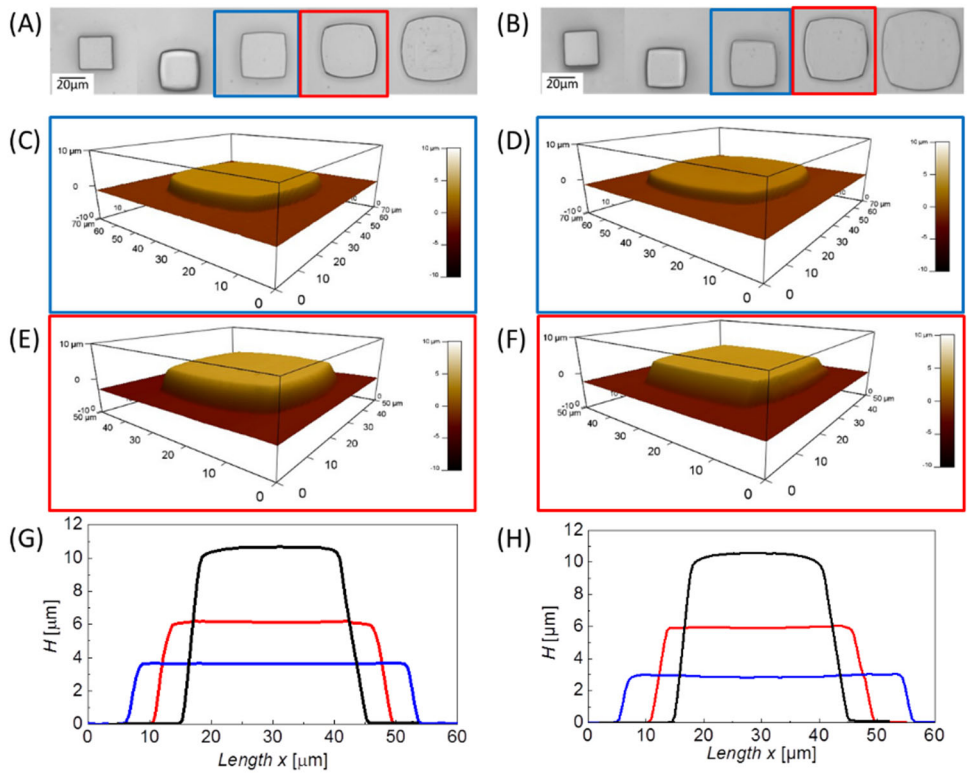

Figure 3: (A, B) Representative optical microscopy images of four cPEVA18 microcuboids (A) original and programmed at 100 ºC to different *CR*s, 27 ± 4% (CR_{27}), 42 ± 1% (CR_{42}), 66 ± 1% (CR_{66}) and 75 ± 1% (CR_{75}) as well as cPEVA40 micro-cuboids (B) original and programmed at 70 ºC to different *CR*s of 23 ± 4% (CR_{23}), 44 ± 1% (CR_{44}), 73 ± 1% (CR_{73}) and 79 ± 1% (CR_{79}). The compression ratio around ~40% and ~70% is framed in blue and red. (C-F) Representative atomic force microscopy 3D height images of two cPEVA18 microcuboids programmed at 100 ºC to different *CR*s: CR_{42} (C) and CR_{66} (E) as well as cPEVA40 micro-cuboids programmed at 70 ºC to different *CR*s: CR_{44} (D) and CR_{73} (F); (G, H) Representative atomic force microscopy height profiles of three cPEVA18 microcuboids (G) original (black)

and programmed at 100 ºC to different *CR*s: CR_{42} (red) and CR_{66} (blue) and as well as cPEVA40 microcuboids (H) original (black) and programmed at 70 ºC to different *CR*s: CR_{44} (red) and CR_{73} (blue).

For AFM, two *CR* which gave most distinguishable results (red and blue frame in **Figure 3**) were selected and were used for further analysis in this study, if not somewhere else mentioned (additional data are available in the Supporting information).

Microcuboids programmed to different compression ratios were selected to explore the influence of the degree of deformation on the dual-shape performance of the cPEVA cuboids. The microlevel recovery of the cuboids was first analyzed by OM. In OM experiments the shape change of the cuboids was monitored while heating from 25 °C to 100 °C for cPEVA18 or 25 °C to 80 °C for cPEVA40 and was followed by the change in *PA* (see **Supporting Information, Figure S1**)**.** In Figure 4A the temperature dependent recovery of cPEVA18 microcuboids deformed to CR_{42} and CR_{66} are shown (for CR_{27} and CR_{75} see **Supporting Information, Figure S2A)**, while Figure 4C depicts the recovery for cPEVA40 microcuboids deformed at similar compression ratios – CR_{44} and CR_{73}. An almost complete recovery of the respective *PA* could be observed for cPEVA18 microcuboids with CR_{27}, and only a partial recovery was achieved for microcuboids with higher *CR* values. Similar changes in the *PA*s were monitored during the recovery experiments. The *PA* of 2135 ± 63 μm^2 (CR_{75}) for cPEVA18 at 25 °C was decreased to *PA* = 920 ± 20 μm^2 at 100 °C, indicating a partial recovery while the *PA* of 730 ± 25 μm^2 (CR_{27}) for cPEVA18 at 25 °C was decreased to *PA* = 522 ± 20 μm^2 at 100 °C, showing an almost complete recovery of the original PA. Comparably, cPEVA40 microcuboids showed a lower recovery throughout the *CR* series to the original shape.

As quantitative measure of the first level (micro) of the dual-shape performance of a material the shape recovery ratio ($R_{r,micro}$) can be calculated according to equation (5), where H_0 is the

original height, H_u is the temporary fixed height, and H_p is the recovered height determined by AFM experiments.

$$R_{r,micro} = \frac{H_p - H_u}{H_0 - H_u} \times 100\% \quad (5)$$

A slight decrease in $R_{r,micro}$ of cPEVA18 microcuboids from 102 ± 1% to 93 ± 1% was observed when *CR* increased from CR_{42} to CR_{66}, demonstrating the influence of the degree of compression applied during programming. However, a significant influence of compression degree on $R_{r,micro}$ was observed for cPEVA40 microcuboids where R_r decreased from 88 ± 1% to 42 ± 1% with increasing *CR* from CR_{44} to CR_{73}. Furthermore, a higher compression ratio would result in a higher contribution of irreversible deformation, which might be related to an enhanced adhesion to the glass substrate that prevents a complete recovery.

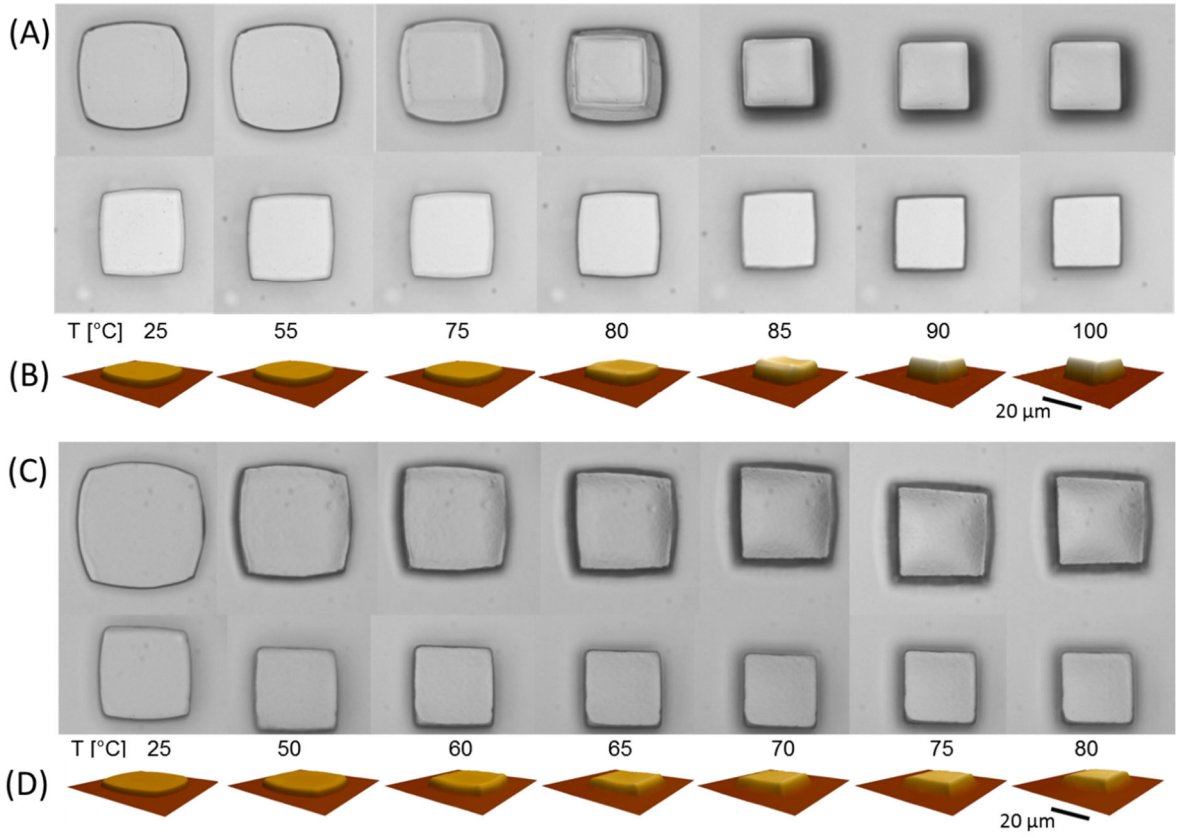

Figure 4: (A,C) Representative optical microscopy images of the shape recovery during heating from 25 to 100 °C for cPEVA18 microcuboids (A) programmed at 100 ºC to two different *CR*s: CR_{42} (lower series in A) and CR_{66} (top series in A), as well as from 25 to 80 ºC for two cPEVA40 microcuboids (C) programmed at 70 ºC to two different *CR*s: of CR_{44} (lower series in C) and CR_{73} (top series in C); (B, D) Representative AFM 3D height images of the

shape recovery during heating from 25 to 100 °C for two cPEVA18 microcuboids (B) programmed at 100 ºC to CR_{66}, as well as from 25 to 80 ºC for two cPEVA40 microcuboids (D) programmed at 70 ºC to CR_{73}.

Further kinetic investigations of cuboids, recording the change of PA by an OM, were carried out (see **Supporting Information Figure S3**). Interestingly analyzing the respective normalized area change over the time a two-step process is recognized, which can be divided into a very fast recovery process occurring almost instantaneously after exposure to the elevated temperature within the first few seconds, followed by a slow recovery process which is completed after several minutes (**Figure 5**). Applying an expanded exponential fit (see Experimental Section), two individual τ values of 1.5 s and 129 s for cPEVA40 and 12.2 s and 303 s for cPEVA18 are obtained. Here, cPEVA40 exhibited a much faster initial decay of PA when compared to cPEVA18, which might be attributed to the lower melting transition. In contrast, the second, slow change in PA until the recovery process completed recovery is in a similar range for both materials. The first step of recovery was assigned to the release of the majority of stored stress which leads to an instantaneous change throughout the cuboid overcoming the competing adhesive forces. The following (much slower) recovery process represents the entropy driven shape change of cuboids which are in an almost rubbery elastic state modulated by the adhesion to the surface until an equilibrium is reached and the recovery is completed.

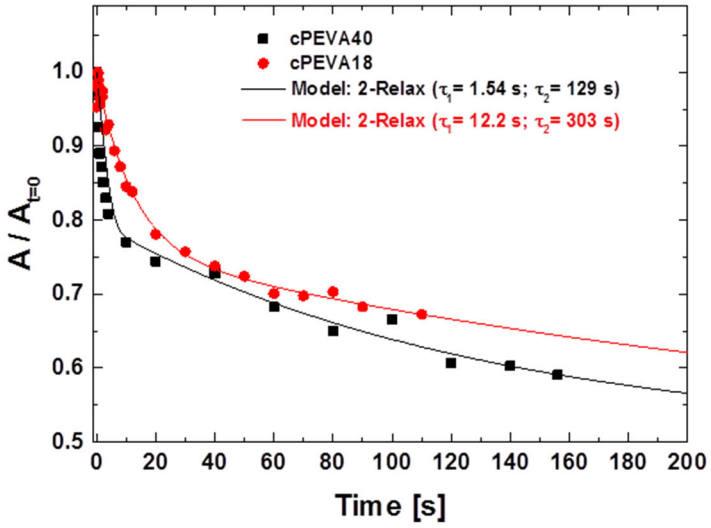

Figure 5: Comparison of kinetic normalized area changes obtained by *OM* over time for cPEVA18 (red spheres) and cPEVA40 (black squares) recorded at 100 °C. Data were fitted by an expanded exponential fit indicating two distinguish recovery rates.

In situ AFM recovery experiments were conducted with cPEVA18 microcuboids having a CR_{42} ($H_u = 6.2 \pm 0.1$ µm) and CR_{66} ($H_u = 3.6 \pm 0.1$ µm) as well as cPEVA40 microcuboids having a CR_{44} ($H_u = 5.9 \pm 0.1$ µm) and CR_{73} ($H_u = 2.8 \pm 0.1$ µm). In **Figures 6 B, D and Figure S2, Supplementary Information**, the 3D height images recorded at different temperatures are presented. Both cPEVA18 microcuboids reached similar heights of $H = 10.7 \pm 0.1$ µm or $H = 10.9 \pm 0.1$ µm, which is slightly above the height determined for the original microcuboids ($H = 10.8 \pm 0.1$ µm) (**Figures 6A, B**). For cPEVA40 microcuboids, full recovery was reached to $H = 9.9 \pm 0.1$ µm with CR_{44} and only partial recovery was observed to $H = 6.1 \pm 0.1$ µm with CR_{73} (**Figures 6D, E**). From such height profiles it becomes obvious that the cPEVA18 sample with CR_{42} exhibited an almost homogeneous change in height H with raising temperature, whereby higher H values were obtained at the edges of the microcuboids when compared to the central region. This difference might be related to a nonuniform distribution of strain direction during programming of the microcuboids. A similar recovery behavior was found for the cPEVA18 sample with CR_{66}, but here a slightly tilted recovered surface was achieved. The

cPEVA40 sample with CR_{44}, exhibited a homogeneous, complete recovery in height H with raising temperature. In contrast cPEVA40 with CR_{73} recovered to a curved surface differing from the original flat face.

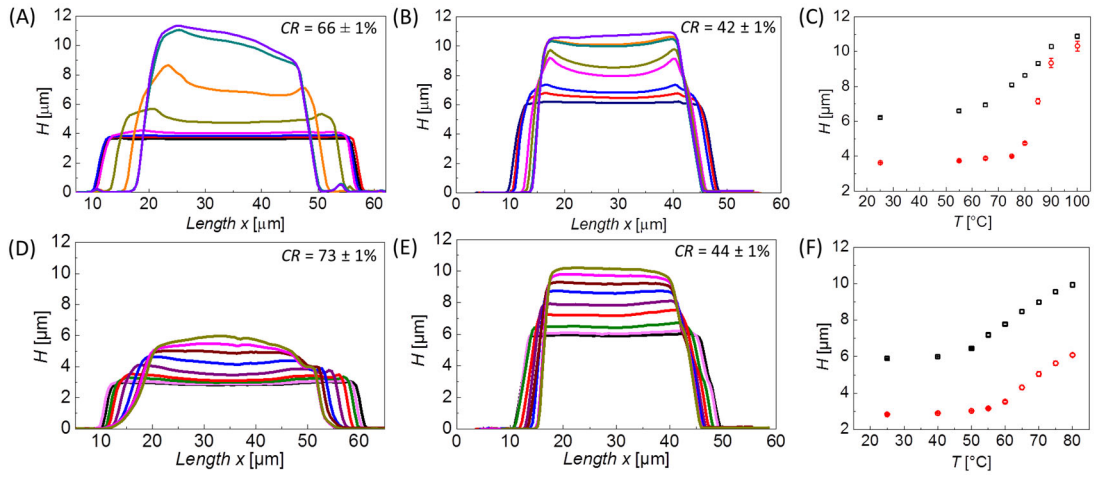

Figure 6: (A, B) Changes in microcuboid height profiles obtained by AFM during heating from 25 to 100 °C for cPEVA18 microcuboids CR_{66} (A) and CR_{42} (B): Color represents different temperatures: 25 °C (black), 55 °C (red), 65 °C (blue), 75 °C (magenta), 80 °C (dark yellow), 85 °C (orange), 90 °C (dark cyan), and 100 °C (violet). (D, E) Changes in microcuboid height profiles obtained by AFM during heating from 25 to 80 °C for cPEVA40 microcuboids CR_{73} (D) and CR_{44} (E): Color represents different temperatures: 25 °C (black), 40°C (LT magenta), 50°C (olive), 55 °C (red), 60 °C (purple), 65 °C (blue), 70°C (wine), 75 °C (magenta), and 80 °C (dark yellow). (C, F) Shape recovery H vs. temperature curves of cPEVA18 microcuboids (C) with CR of 42 ± 1% (black) and 66 ± 1% (red) as well as cPEVA40 micro-cuboids (F) with CR of 44 ± 1% (black) and 73 ± 1% (red).

The switching temperature T_{sw} of both cPEVAs microcuboids can be determined from the inflection point of the H versus temperature recovery curves, which are displayed in **Figures 6C and F**. For cPEVA18, similar T_{sw} of 83 ± 2 °C for CR_{42} and 85 ± 2 °C for CR_{66} were obtained. Significant lower switching temperatures were found for cPEVA40 with T_{sw} = 63 ± 2 °C (CR_{44}) and 68 ± 2 °C (CR_{73}), indicating similar shape-recovery kinetics for microcuboids programmed with different compression ratios. However, the difference in T_{sw} of cPEVA18 and cPEVA40 indicates that T_{sw} can be adjusted by the chemical composition of the material. The shape-memory characteristics are listed in **Table 2**.

3.3 Nano shape-memory capability

Besides the microscale shape recovery characterization of the programmed microcuboids, the nanoscale changes in the surface roughness were also analyzed by AFM measurement. The surface roughness, defined by the root-mean-square roughness ($R_{q(0)}$), of the original microcuboids top face, which were in direct contact with the PDMS mold microcavities was 17 ± 1 nm for cPEVA18 and 19 ± 1 nm for cPEVA40. This particular R_q originated from the etching process applied for preparation of the microstructured Si-wafer, which was utilized as template for generation of the PDMS mold.[38] To exclude any disturbing effect, only samples with a low compression state were chosen for investigations. A reduction of surface roughness to $R_{q(u)}$ = 5 ± 1 nm for cPEVA18 (CR_{42}) and $R_{q(u)}$ = 8 ± 2 nm for cPEVA40 (CR_{44}) was found in the programmed microcuboids. This indicates that the smooth surface of the glass plate was programmed to the top surface of microcuboids during compression and was determined by $R_{q(g)}$ = 5 ± 1 nm of glass slide. The fixity ratio $R_{f,nano}$ of the surface roughness on the nanolevel is determined according to the following equation (6):

$$R_{f,\,nano} = \frac{R_{q(0)} - R_{q(u)}}{R_{q(0)} - R_{q(g)}} \cdot 100\% \qquad (6)$$

An excellent fixity ($R_{f,nano}$) was achieved in cPEVA18 as 100 ± 8% and cPEVA40 reached a lower fixity ratio of 79 ± 14%. In contrast to thermoplastic polymers, which tend to erase their surface features at elevated temperature due to minimizing surface energy, the surface roughness of the crude cuboids stayed almost the same with 23 ± 5 nm for cPEVA18 and 22 ± 1 nm for cPEVA40 during heating as shown in **Figures 7A, B**. The nanosurface increased to the original level during recovery of the microcuboids with $R_{q(p)}$ = 21 ± 1 nm for cPEVA18 and $R_{q(p)}$ = 27 ± 3 nm for cPEVA40 (**Figures 7C, D**). Similar to $R_{r,\,micro}$, the recovery ratio of surface roughness $R_{r,\,nano}$ is characterized by following equation (7), $R_{q(p)}$ is the recovered roughness.

$$R_{r,\,nano} = \frac{R_{q(p)} - R_{q(u)}}{R_{q(0)} - R_{q(u)}} \times 100\% \qquad (7)$$

$R_{r,\,nano}$ of cPEVA18 was calculated as 89 ± 6% and for cPEVA40 was 136 ± 21% (Table 2). According to the recovery kinetics discussed for the $R_{r,micro}$, it is assumed that the recovery of the nanoroughness can be assigned to the fast recovery process which occurs instantaneously. The AFM height images presenting the surface center of programmed cPEVA microcuboids during heating are shown in **Figure 7**.

Table 2. Shape-memory characteristics of cPEVA18 and cPEVA40 microcuboids determined by AFM

Material	CR[a] [%]	$R_{r,\,micro}$[b] [%]	$R_{f,\,nano}$[c] [%]	$R_{r,\,nano}$[d] [%]	T_{sw}[e] [°C]
cPEVA18	42 ± 1	102 ± 1	100 ± 8	89 ± 6	83 ± 2
	66 ± 1	93 ± 1	-	-	85 ± 2
cPEVA40	44 ± 1	88 ± 1	79 ± 14	136 ± 21	63 ± 2
	73 ± 1	42 ± 1	-	-	68 ± 2

[a]compression rate, [b]recovery ratio of microcuboids, [c]fixity ratio of the nano-roughness, [d]recovery ratio of the nano-roughness [e]switching temperature.

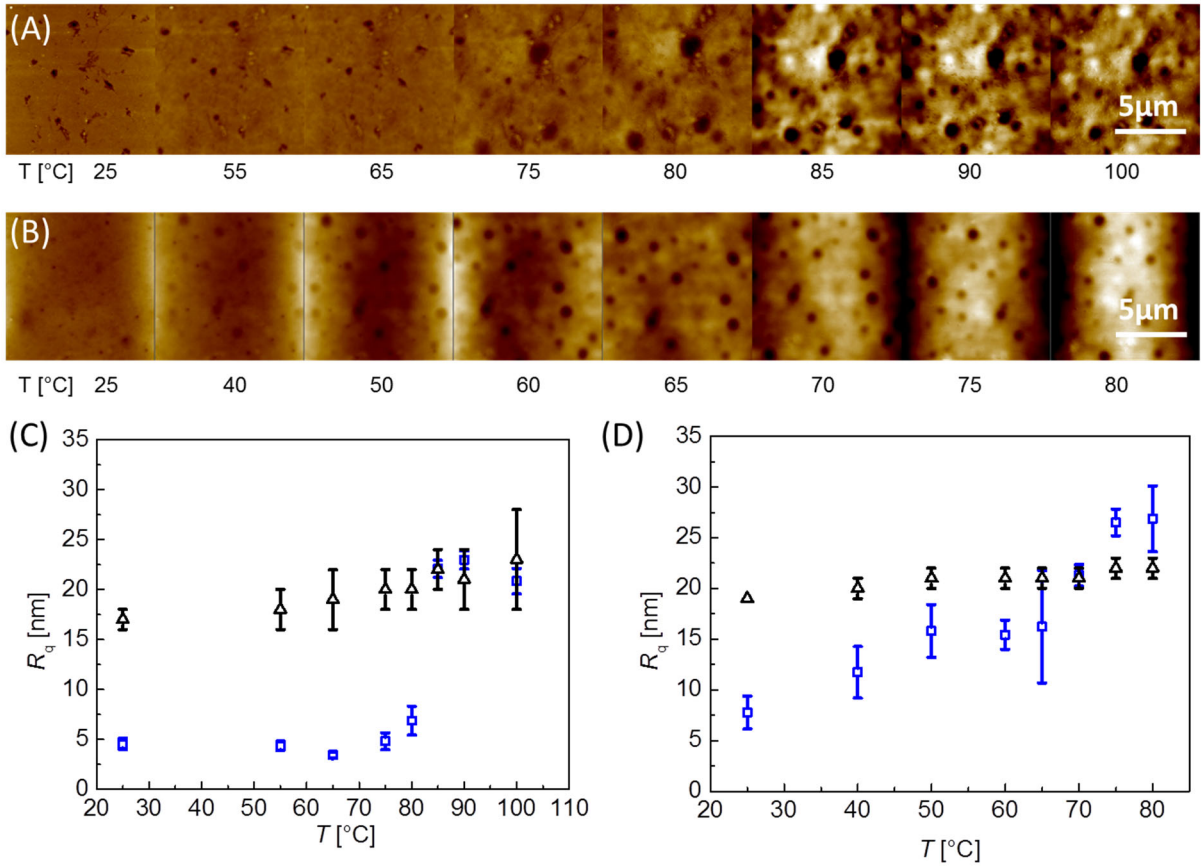

Figure 7: (A, B) Representative height images presenting the top surface center of programmed cPEVA18 (A) during increasing temperature from 25 to 100 °C and cPEVA40 (B) during increasing temperature from 25 to 80 °C. The contrast of height image is from -50 nm to 50 nm. (C, D) Surface roughness change with increasing temperature of cPEVA18 (C) programmed (blue squares) or original (black triangles) microcuboids and cPEVA40 (D) programmed (blue squares) or original (black triangles) microcuboids.

4. Conclusions

In summary, cPEVA18 and cPEVA40 based microcuboids were successfully fabricated by a soft lithography approach. Programming by compression resulted in various deformed micro-cuboids exhibiting compression ratios (*CR*) ranging from 27 ± 4% to 75 ± 1% for cPEVA18 and from 23 ± 4% to 79 ± 1% for cPEVA40. The temperature driven shape recovery of differently programmed microcuboids was examined by optical microscopy and *in situ* AFM experiments. Excellent shape-memory properties on the micro-level, characterized by a complete recovery of the original microcuboid dimensions independent from the compression

ratio were achieved in AFM investigations. In contrast, the shape recovery monitored by optical microscopy could show an influence of the applied compression ratio on the shape recovery ratio. All investigated microcuboids exhibited similar switching temperatures in the range from 83 to 85 °C for cPEVA18 and between 63 and 68 °C for cPEVA40 for different *CR*s. Along with the programming and recovery of the microscaled cuboids, surface features on the nano-scale level at their top face were studied by AFM. The surface roughness (R_q) of the cuboids was recovered to the origin level after programming by compression. The presented microcuboids showing micro- and nanoscale changes in shape can be useful for side specific self-assembly, enhanced interaction with cells or alteration of the rheological properties of suspensions.[36] Here, cPEVA was used as a generalized system for preparing microcuboids and their two-level recovery was monitored via a combination of methods. However, more precise microcuboids with well-defined geometries and nanopatterned surface can be fabricated by using specific substrates with structured surfaces during programming. Furthermore, tailorable shapes of the microcuboids depending on the new applications can be envisioned.

Supporting information

The Supporting Information is available free of charge on the ACS Publications website at DOI: 10.1021/acs.macromol.6b02237.

Series of optical microscopy images and 3D height images obtained by atomic force microscopy for cPEVA18 and cPEVA40 microcuboids during heating; shape recovery analysis of cPEVA microcuboids concerning the temperature dependent *PA* development.

Funding

This work was supported by the Helmholtz-Association through program-oriented funding, Y. L. acknowledges financial support by the German Federal Ministry for Education and Research (MIE project, Grant No.031A095).

References

1. Fleischmann, E.-K.; Forst, F. R.; Koder, K.; Kapernaum, N.; Zentel, R. Microactuators from a main-chain liquid crystalline elastomer via thiol-ene "click" chemistry. *J. Mater. Chem. C* **2013,** 1 (37), 5885-5891.
2. Ohm, C.; Serra, C.; Zentel, R. A Continuous Flow Synthesis of Micrometer-Sized Actuators from Liquid Crystalline Elastomers. *Adv. Mater. (Weinheim, Ger.)* **2009,** 21 (47), 4859-4862.
3. Ilievski, F.; Mazzeo, A. D.; Shepherd, R. E.; Chen, X.; Whitesides, G. M. Soft Robotics for Chemists. *Angew. Chem., Int. Ed.* **2011,** 50 (8), 1890-1895.
4. Friess, F.; Nöchel, U.; Lendlein, A.; Wischke, C. Polymer Micronetworks with Shape-Memory as Future Platform to Explore Shape-Dependent Biological Effects. *Adv. Healthcare Mater.* **2014,** 3 (12), 1986-1990.
5. Takeda, I.; Kawanabe, M.; Kaneko, A. An investigation of cell adhesion and growth on micro/nano-scale structured surface—Self-assembled micro particles as a scaffold. *Precis. Eng.* **2016,** 43, 294-298.
6. Liu, S.; Deng, R.; Li, W.; Zhu, J. Polymer Microparticles with Controllable Surface Textures Generated through Interfacial Instabilities of Emulsion Droplets. *Adv. Funct. Mater.* **2012,** 22 (8), 1692-1697.
7. Choi, C. H.; Lee, B.; Kim, J.; Nam, J. O.; Yi, H.; Lee, C. S. Controlled Fabrication of Microparticles with Complex 3D Geometries by Tunable Interfacial Deformation of Confined Polymeric Fluids in 2D Micromolds. *ACS Appl. Mater. Interfaces* **2015,** 7 (21), 11393-11401.
8. Diller, E.; Sitti, M. Three-Dimensional Programmable Assembly by Untethered Magnetic Robotic Micro-Grippers. *Adv. Funct. Mater.* **2014,** 24 (28), 4397-4404.
9. Zhou, J.; Turner, S. A.; Brosnan, S. M.; Li, Q.; Carrillo, J.-M. Y.; Nykypanchuk, D.; Gang, O.; Ashby, V. S.; Dobrynin, A. V.; Sheiko, S. S. Shapeshifting: Reversible Shape Memory in Semicrystalline Elastomers. *Macromolecules* **2014,** 47 (5), 1768-1776.
10. Blum, A. P.; Kammeyer, J. K.; Rush, A. M.; Callmann, C. E.; Hahn, M. E.; Gianneschi, N. C. Stimuli-Responsive Nanomaterials for Biomedical Applications. *J. Am. Chem. Soc.* **2015,** 137 (6), 2140-2154.
11. Mura, S.; Nicolas, J.; Couvreur, P. Stimuli-responsive nanocarriers for drug delivery. *Nat. Mater.* **2013,** 12 (11), 991-1003.
12. Kratz, K.; Madbouly, S. A.; Wagermaier, W.; Lendlein, A. Temperature-Memory Polymer Networks with Crystallizable Controlling Units. *Adv. Mater. (Weinheim, Ger.)* **2011,** 23 (35), 4058-4062.
13. Jochum, F. D.; Theato, P. Temperature- and light-responsive smart polymer materials. *Chem. Soc. Rev.* **2013,** 42 (17), 7468-7483.
14. Mendez, J.; Annamalai, P. K.; Eichhorn, S. J.; Rusli, R.; Rowan, S. J.; Foster, E. J.; Weder, C. Bioinspired Mechanically Adaptive Polymer Nanocomposites with Water-Activated Shape-Memory Effect. *Macromolecules* **2011,** 44 (17), 6827-6835.
15. Felber, A. E.; Dufresne, M.-H.; Leroux, J.-C. pH-sensitive vesicles, polymeric micelles, and nanospheres prepared with polycarboxylates. *Adv. Drug Delivery Rev.* **2012,** 64 (11), 979-992.
16. Tanaka, Y.; Fujikawa, T.; Kazoe, Y.; Kitamori, T. An active valve incorporated into a microchip using a high strain electroactive polymer. *Sens. Actuators, B* **2013,** 184, 163-169.
17. Li, Q.; Zhou, J.; Vatankhah-Varnoosfaderani, M.; Nykypanchuk, D.; Gang, O.; Sheiko, S. S. Advancing Reversible Shape Memory by Tuning the Polymer Network Architecture. *Macromolecules* **2016,** 49 (4), 1383-1391.

18. Leite, A. J.; Caridade, S. G.; Mano, J. F. Synthesis and characterization of bioactive biodegradable chitosan composite spheres with shape memory capability. *J. Non-Cryst. Solids* **2016,** 432, 158-166.
19. Xiao, X.; Kong, D.; Qiu, X.; Zhang, W.; Zhang, F.; Liu, L.; Liu, Y.; Zhang, S.; Hu, Y.; Leng, J. Shape-Memory Polymers with Adjustable High Glass Transition Temperatures. *Macromolecules* **2015,** 48 (11), 3582-3589.
20. Zhao, Q.; Qi, H. J.; Xie, T. Recent progress in shape memory polymer: New behavior, enabling materials, and mechanistic understanding. *Prog. Polym. Sci.* **2015,** 49-50, 79-120.
21. Raidt, T.; Hoeher, R.; Meuris, M.; Katzenberg, F.; Tiller, J. C. Ionically Cross-Linked Shape Memory Polypropylene. *Macromolecules* **2016,** 49 (18), 6918-6927.
22. Bae, W. G.; Choi, J. H.; Suh, K. Y. Pitch-Tunable Size Reduction Patterning with a Temperature-Memory Polymer. *Small* **2013,** 9 (2), 193-198.
23. Jiang, Y.; Fang, L.; Kratz, K.; Lendlein, A. Influence of Compression Direction on the Shape-Memory Effect of Micro-Cylinder Arrays Prepared from Semi-Crystalline Polymer Networks. *MRS Adv.* **2016,** 1 (27), 1985-1993.
24. Xu, H.; Yu, C.; Wang, S.; Malyarchuk, V.; Xie, T.; Rogers, J. A. Deformable, Programmable, and Shape-Memorizing Micro-Optics. *Adv. Funct. Mater.* **2013,** 23 (26), 3299-3306.
25. Karger-Kocsis, J.; Keki, S. Biodegradable polyester-based shape memory polymers: Concepts of (supra)molecular architecturing. *eXPRESS Polym. Lett.* **2014,** 8 (6), 397-412.
26. Gong, T.; Lu, L.; Liu, D.; Liu, X.; Zhao, K.; Chen, Y.; Zhou, S. Dynamically tunable polymer microwells for directing mesenchymal stem cell differentiation into osteogenesis. *J. Mater. Chem. B* **2015,** 3 (46), 9011-9022.
27. Gong, T.; Zhao, K.; Liu, X.; Lu, L.; Liu, D.; Zhou, S. A Dynamically Tunable, Bioinspired Micropatterned Surface Regulates Vascular Endothelial and Smooth Muscle Cells Growth at Vascularization. *Small* **2016,** 12 (41), 5769-5778.
28. Gong, T.; Zhao, K.; Wang, W.; Chen, H.; Wang, L.; Zhou, S. Thermally activated reversible shape switch of polymer particles. *J. Mater. Chem. B* **2014,** 2 (39), 6855-6866.
29. Cox, L. M.; Killgore, J. P.; Li, Z. W.; Long, R.; Sanders, A. W.; Xiao, J. L.; Ding, Y. F. Influences of Substrate Adhesion and Particle Size on the Shape Memory Effect of Polystyrene Particles. *Langmuir* **2016,** 32 (15), 3691-3698.
30. Wang, J.-T.; Wang, J.; Han, J.-J. Fabrication of Advanced Particles and Particle-Based Materials Assisted by Droplet-Based Microfluidics. *Small* **2011,** 7 (13), 1728-1754.
31. Brosnan, S. M.; Jackson, A.-M. S.; Wang, Y.; Ashby, V. S. Shape Memory Particles Capable of Controlled Geometric and Chemical Asymmetry made from Aliphatic Polyesters. *Macromol. Rapid Commun.* **2014,** 35 (19), 1653-1660.
32. An, Y. H.; Friedman, R. J. Concise review of mechanisms of bacterial adhesion to biomaterial surfaces. *Journal of Biomedical Materials Research* **1998,** 43 (3), 338-348.
33. Quere, D. Wetting and roughness. *Annu. Rev. Mater. Res.* **2008,** 38, 71-99.
34. Smith, M. A.; Zoelle, A.; Yang, Y.; Rioux, R. M.; Hamilton, N. G.; Arnakawa, K.; Nielsen, P. K.; Trunschke, A. Surface roughness effects in the catalytic behavior of vanadia supported on SBA-15. *J. Catal.* **2014,** 312, 170-178.
35. Guan, J. J.; Ferrell, N.; Lee, L. J.; Hansford, D. J. Fabrication of polymeric microparticles for drug delivery by soft lithography. *Biomaterials* **2006,** 27 (21), 4034-4041.
36. Audus, D. J.; Hassan, A. M.; Garboczic, E. J.; Douglas, J. F. Interplay of particle shape and suspension properties: a study of cube-like particles. *Soft Matter* **2015,** 11 (17), 3360-3366.
37. Wischke, C.; Lendlein, A. Method for Preparation, Programming, and Characterization of Miniaturized Particulate Shape-Memory Polymer Matrices. *Langmuir* **2014,** 30 (10), 2820-2827.

38. Xu, X.; Wang, W. W.; Kratz, K.; Fang, L.; Li, Z. D.; Kurtz, A.; Ma, N.; Lendlein, A. Controlling Major Cellular Processes of Human Mesenchymal Stem Cells using Microwell Structures. *Adv. Healthcare Mater.* **2014,** 3 (12), 1991-2003.